Journal of NeuroEngineering and Rehabilitation

RESEARCH

Open Access

A patient-specific, 3D printed neurostimulator enabling focal transcranial electrical stimulation and EEG at home

Mahyar Joodaki[1], Griffin Rodgers[1,2], Alois Hopf[1*], Mathias R. Koller[1], Raphael Guzman[3], Emiliano Santarnecchi[4,5], Johannes S. Vögerl[6], Julian Ferchow[7], Annina Ruffner[1], Marc Funken[1], Mirko Meboldt[6] and Bekim Osmani[1,2]

Abstract

Background The therapeutic potential of non-invasive transcranial electric stimulation (tES) is growing, but challenges in tailoring treatments to individual patients persist. We demonstrated that personalized montages, informed by biophysical modeling, can reduce dose variability and improve target engagement. However, traditional setups are prone to electrode placement errors, leading to inconsistent dosage, localization and potential off-target engagement.

Methods We developed a pipeline for creating patient-specific 3D-printed caps based on individual MRI scans to allow custom placement of up to 34 electrodes. Hybrid brush electrodes were incorporated to facilitate the use on with-hair regions of the head. The patient-specific caps are integrated within a Neurostimulator/EEG device, enabling precise electrode placement for recording of neural activity and optimized, personalised tES therapies based on individual biophysical brain models.

Results A proof-of-concept in-silico study highlighted the importance of positional accuracy in electrode placement, particularly in minimizing off-target stimulation in case of the personalized montage configuration. To mitigate positional displacement, we introduced the pipeline for generating patient-specific 3D-printed caps, ensuring precise anatomical fit. The flexible design of these caps supports high-density electrode arrays tailored to various therapeutic montages. Integrated brush electrodes function in both dry and wet modes and are powered by electronics embedded in a neckpiece, enabling multi-step tES and EEG recording with minimal setup for at-home use. Electrical and mechanical evaluations confirmed the system's feasibility, and a clinical trial with eight healthy subjects showed improved comfort and increased willingness for home use.

Conclusion This customized cap-electrode system provides a practical solution for self-administered, repeatable personalized tES and EEG session at home.

Trial registration: The study is registered on the Swiss National Clinical Trials Portal (SNCTP), (SNCTP000005598) and Clinicaltrials.gov (NCT05999916). The study was approved by the Independent Competent Ethics Committee

*Correspondence:
Alois Hopf
Alois.hopf@bottneuro.ch

Full list of author information is available at the end of the article

(Ethikkommission Nordwest-und Zentralschweiz (EKNZ)) at the 14 August 2023 and the Competent Regulatory Authority Swissmedic at the 20 December 2023.

Introduction

Transcranial electric stimulation (tES) is emerging as a promising non-invasive therapeutic approach for various neurodegenerative and psychiatric disorders [1–3]. While transcranial direct current stimulation (tDCS) has gained commercial availability, particularly for the treatment of depression [4], transcranial alternating current stimulation (tACS) remains predominantly applied within research settings [5–7]. Recent clinical trials have shown encouraging results for tACS in addressing complex conditions such as Alzheimer's disease [8–10]. However, the therapeutic application of tES remains challenging, as different disorders demand varying electrode configurations and levels of precision in targeting [11]. Hence, neurostimulation devices must meet several criteria: (i) flexible, personalized electrode placement for montages that maximize target engagement for a wide range of anatomies and therapeutic applications, (ii) accurate electrode positioning across multiple sessions, and (iii) easy set-up and use to minimize human errors and enable long-term home use over weeks or months.

One of the challenges in tES therapy is to enhance the localization of the induced electric fields at the region of interest (ROI) and minimize stimulation of adjacent areas. High definition (HD) montages are recognized for their high focality; however, this advantage often comes at the expense of inconsistent stimulation dosage between subjects as a result of the fixed electrode positions and standard current per electrode that do not account for inter-subject morphological differences. To accurately predict which region receives stimulation in live tissues, physical simulations are indispensable [12]. To that end, recent advances using personalized, multilayer 3D head models derived from Magnetic Resonance Images (MRI) have significantly improved simulation precision by accounting for inter-individual morphological differences [13]. In addition, optimization methods have been used to improve on standardized montages, identifying the most effective montage configurations to ensure adequate dose delivery to a given ROI and reduce off-target stimulation [14, 15]. By incorporating physical limitations – such as maximum current per electrode and maximum total current – as tunable parameters into optimization algorithms, proposed montages can comply with device specifications and safety limits [16]. Increasing the number and density of available electrodes generally enhances montage optimization results for cortical ROIs [16]. For targeting deep brain ROIs more sophisticated methods including temporal interference have shown promising results [17–19]. Flexible and dense electrode placement is thus important for tES, though many available devices are either restricted to 32 predefined positions or offer flexibility at the cost of complex set up and operation that requires assistance.

Consistency in stimulation dosage is crucial for tES-based therapies: first, with increased interest in the clinical efficacy of tES, minimizing variability between subjects – both in terms of on- and off-target dose – is essential for the validity and reproducibility of tES studies. Second, maintaining the stimulation dosage above the therapeutic threshold is key to effective treatment outcomes [20, 21]. Since tES is typically administered across multiple sessions rather than as a single intervention [6, 22], consistency in dosage and electrode placement across sessions is a prerequisite for reliable therapeutic results [23]. Currently, biophysical simulations are the most reliable method for predicting tES-induced electric field distributions in the brain, making them invaluable for therapy planning. However, even the most precise simulations encounter errors during practical implementation, particularly when standard, one-size-fits-all caps are used for electrode placement [24]. Inconsistency in electrode placement over repeated use can lead to variability in stimulation location and dosage [25, 26]. This is especially relevant in light of the growing understanding of the functional connectivity of neighboring regions and their correlations and anticorrelations, which necessitates avoiding simultaneous stimulation of different and potentially neighboring regions [27–29]. Although there are recommendations to improve the electrode positioning accuracy in practice [30–32], these approaches are often unsuitable for home-use medical devices – particularly for multi-electrode personalized montages – due to their complexity and the associated risk of user error. Among these, 3D-printed headset developed as form-fitted, MRI-free headsets for rTMS has offered an intermediate approach between heuristic placement and MRI-guided navigation [33]. Consequently, home-use systems typically require supervision, which is generally only feasible in clinical trial settings [34, 35]. To enhance the usability and accessibility of neuromodulation therapy for independent home use, simplified device designs have been introduced. These designs often involve reducing electrode placement to two fixed locations and increasing electrode size, thereby minimizing setup complexity and the potential for user error at the expense of inter-subject dose variability and losing dose localization [4, 36, 37].

A similar need for consistency and accuracy applies to Electroencephalogram (EEG) monitoring. While EEG

recordings are gaining attention for brain-computer interface applications, regular EEG monitoring is increasingly used to observe brain activity for various purposes. These include tracking psychiatric and neurological disorders [38, 39], assessing the efficacy of neurostimulation therapies [40, 41], closed-loop tACS therapy for personalized stimulation phase and frequency [42, 43], and personalized targeting for tDCS [44]. Furthermore, studies demonstrated that the increased brain activity in the tACS frequency band correlates with the stimulation site [45] and it is often observed in post-therapy EEG recordings taken from the same electrodes used for tES [46]. As a result, integrated tES-EEG systems are desirable [47].

Ensuring proper electrode-to-scalp contact, particularly in hair-covered regions, further complicates the administration of both tES and EEG, often necessitating the use of conductive gels or saline [47]. While various designs have been proposed for dry or semi-dry electrodes [48–50], most are optimized for EEG recordings rather than tES. Among these, brush-like electrodes are particularly effective on hair-covered regions [51–53]. However, for tES applications, the use of conductive electrolytes is typically unavoidable to increase the contact stability, reduce skin-electrode interfacial impedance and associated sensations during stimulation.

As a solution to these shortcomings of tES devices, we propose a pipeline for generating customized 3D-printed caps tailored to each patient's unique head morphology. We use in silico modelling to demonstrate the advantages of the personally optimized montages over one-size-fits-all approaches and explore the inaccuracies associated with montage displacements. The proposed neurostimulator caps feature personalized electrode positioning, allowing for patient-specific montages for focal tES based on a variety of indications, protocols and targets depending on the patient condition or study design. Additionally, we introduced Ag/AgCl-coated hybrid brush electrodes, designed to be used in both dry and wet mode, specifically engineered for these caps. Finally, the 3D-printed cap and electrodes are incorporated into the neurostimulator equipped with EEG recording electronics embedded in a neckpiece. The electrical and mechanical properties of the system have been experimentally validated, and the device was used in a clinical trial with healthy subjects to assess safety and usability. The custom-made tES neurostimulator and EEG recording device offers a path towards user-friendly, repeatable solutions to deliver at-home therapy without losing spatial accuracy across multiple sessions.

Results

In silico proof-of-concept for positional accuracy

Simulations were based on personalized head models from MRIs of ten healthy subjects participating in MindStim clinical trial (NCT05999916). Figure 1 compares the simulated electric field distributions from HD montages (1:4) using fixed standardized positions and optimized montages using a dense grid electrode positioning system on the same head models. The target ROI for montage optimization was the left angular gyrus with a target electric field intensity of 0.3 V/m. Panel (A) illustrates the electric field magnitude $|\vec{E}|$ distribution for two representative subjects out of ten. Although HD montages yielded focal field distributions of below 1760 mm^2 (the

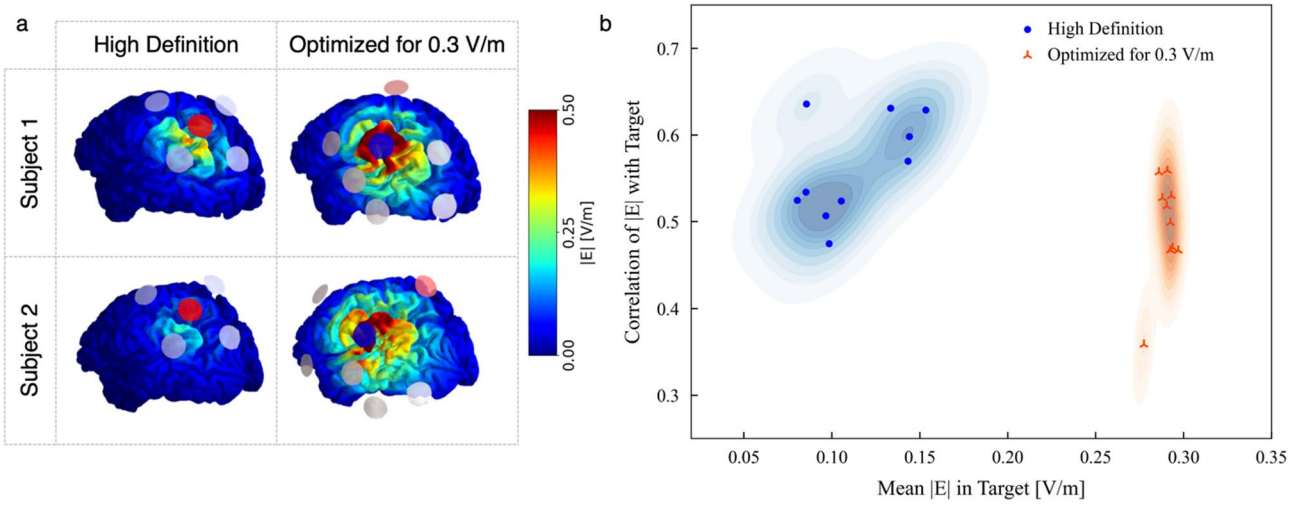

Fig. 1 Customized electrode positioning resolves inter-individual target intensity variability. **a** Electric field magnitude distributions for two subjects with both the fixed HD montage based on the standard 10–20 positioning system (first column) and the optimized montage using a high density positioning system (second column). The target ROI was the left angular gyrus and the target intensity in the ROI was 0.3 V/m. Simulations and optimizations were based on individualized head models extracted from structural MRI. **b** Kernel density estimation (KDE) [54] for correlation of magnitude of electric field |E| with the target ROI vs. mean magnitude of electric field in the ROI for HD (blue) and optimized (orange) montages. Each point in the overlayed scattered plot indicates a subject. The optimized montages had significantly less variation of mean electric field across subjects (Levene's test, $p < 0.05$)

mean surface area of the left angular gyrus target across the subjects) in all cases, the mean magnitude of electric field in ROI $|\bar{E}|_{\mathrm{ROI}}$ was not consistent across subjects and didn't reach the target intensity of 0.3 V/m for any of the subjects. The optimized montages produced more consistent $|\bar{E}|_{\mathrm{ROI}}$ at the mean target intensity of 0.290 ± 0.005 V/m (min-max 0.277–0.297) among all subjects while for HD montages, it's 0.113 ± 0.028 V/m (min-max 0.080–0.153), see Fig. 1b. Optimized montages for the eight subjects showed significantly reduced variance compared to the HD montages, i.e. Levene's test for equality of variances was conducted and showed that the assumption of equal variances was not met, ($F(1, 18) = 12.02$, $p = 0.00275$). For both montages, the correlation of $|\vec{E}|$ with ROI, a surrogate for target engagement, had statically comparable mean and variance (0.56 ± 0.06 for HD and 0.5 ± 0.06 for optimized montages). Thus, optimized montages achieved the desired stimulation intensity across different subjects without substantial loss in target engagement.

In the next experiment, the effect of displacement of a montage was simulated. One subject's optimized montage for the left angular gyrus, showed by green dots in Fig. 2a, was rigidly rotated about the center of the head and the resulting electric fields were calculated. This rotation mimics possible misplacement of a cap on the subject's head, noting that translating/rotating the electrodes together is more representative than independent movement in the case of a rigid cap. The correlation of $|\vec{E}|_{\mathrm{displaced}}$ with $|\vec{E}|_{\mathrm{original}}$ was calculated for each displaced montage (panel b). For displacements beyond 15 mm, (e.g. red montage in panel A and red star in panel b), field distributions showed correlation drop of more than 5% to the original optimized montage for that target, which corresponded to substantial visual differences compared to the desired field distribution and increased off-target magnitudes. Panel c and d show the $\vec{E}$ distribution for the original and displaced montage, respectively, where the misalignment of the cap reduces the correlation with original montage $|\vec{E}|$ intensity by 7% and induce off-target intensities. This displacement also leads to change in $\vec{E}$ direction up to 60°, as shown in panel (d), which can be relevant in cases where the objective is the maximization of electric field normal to the cortical target. Fig. S1 shows the change in target engagement in the form of correlation of $|\vec{E}|$ with the ROI and the change in mean $|\vec{E}|$ in the ROI. Fig. S1 notably illustrate that, in some cases rotated montages exhibit an improved mean $|\vec{E}|$ within the ROI or a stronger correlation with the ROI. Finally, the difference between $|\vec{E}|_{\mathrm{displaced}}$ and $|\vec{E}|_{\mathrm{original}}$ for selected displacements (Fig. S2. c) demonstrates the variability of dosage and, most importantly, increasing off-target intensity due to misplacement of the montage on the subject's head.

Pipeline for design of custom tES/EEG cap

To reduce errors between planned and delivered electric field distributions from a given montage, the electrode positions need to be precisely translated from a 3D head model in digital space to a patient's head in real world space. We propose a solution based on a cap designed for the anatomy of each patient's head as derived from structural MRI scans, see Fig. 3. This pipeline, described in more detail below, consists of five main steps: (1) creating a personalized multilayer 3D model of the entire head, (2) creating an electrode positioning system for each personalized model, (3) positioning electrodes based on prescribed therapy for that patient such as ROI, type of tES/EEG, frequency, required target intensity and any other customization, (4) integrating electrode positions into the cap shell using computer-assisted design (CAD), and (5) adding additional design features to finalize the cap design for 3D printing. The parameters described in the following steps pertain to, but are not limited to, the current version of the tES/EEG hardware.

Head model generation

In the first step, T1-(and optionally T2-) weighted MRI scans with a field-of-view covering entire head and neck are segmented based on tissue type. Currently, we use a 9-component segmentation (white matter, gray mater, cerebrospinal fluid, compact bone, spongy bone, skin, muscles, eyes, blood) compatible with the open-source simulation toolbox SimNIBS [13]. However, if necessary, that can be replaced with more advanced segmentation tools. Further refinements of the segmentation may be needed, particularly in neck region, as the skin surface serves as the reference to ensure a good cap fit. Then, the segmented volume is meshed to create a multi-layer 3D model of the entire head.

Electrode positioning system

In the second step, the rough cap shape, referred to as the cap shell, is created for the head model and the grid of available electrode positions is defined. Electrodes can be flexibly placed in this region, which encompasses the entire cap shell with a 10 mm offset from its outline, preventing electrodes from colliding with the edges of the cap and reducing mechanical stability.

Montage selection

In the third step, the electrode montage is selected based on the patient's prescribed therapy and considering the cap's design constrains such as the minimum distance between electrodes. To avoid electrode-electrode collisions, a minimum electrode spacing is enforced, which

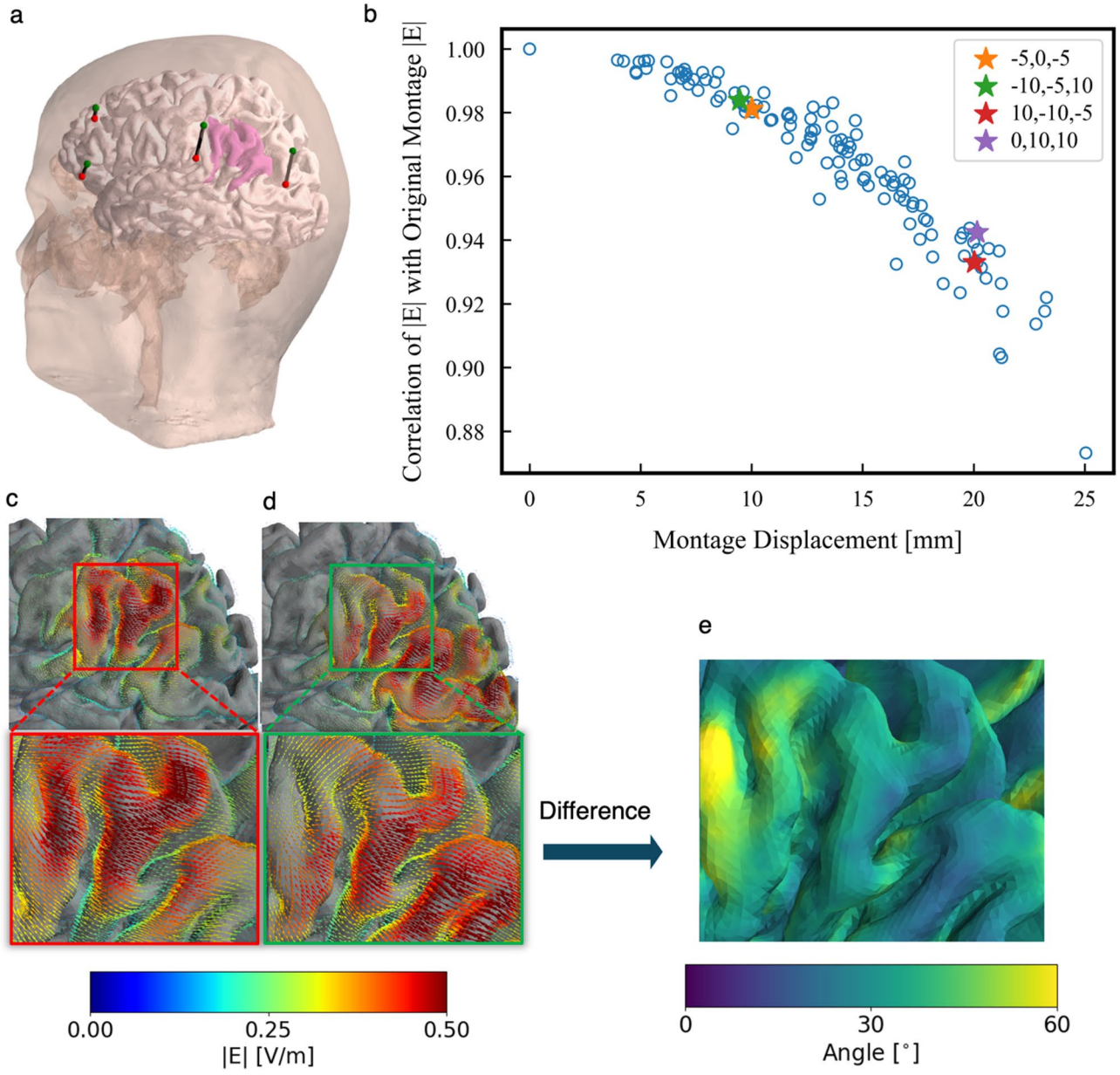

Fig. 2 Displacement of a montage in real-life application shifts stimulation location and electric field orientation. **a** The original montage (green dots) targeting the left angular gyrus (pink area) was displaced via rotations around x, y, z axes (e.g. red dots, where average displacement was 20 mm). **b** Correlation of electric field magnitudes of the displaced montages with the original montage. Each point represents one simulated displaced montage using angle ranges of -10° to 10° about all three axes. **c** and **d** Electric field distributions from the original and displaced montage (red dots and red star, 20 mm displacement), respectively. The color map shows the magnitude of electric fields at each arrow. **e** Difference in angle between electric fields in b and c

is 26.5 mm for the current version of the hardware but can be adapted based on different design features or electrode sizes. For the purposes of cap design, montages can be chosen from a variety of strategies including standardized fixed electrodes, current-adapted fixed electrodes, reference-model optimizations, or fully personalized optimizations or simulations. Given that a personalized head model is necessary, optimized or ad-hoc montages based on patient-specific anatomies and simulations are most suitable. Figure 3 shows an example of a montage with four electrodes optimized for a left angular gyrus target. Current hardware supports up to 8 active electrodes per stimulation step and up to 32 customized positions total for active electrodes. The latter is relevant for multi-step or multi-target therapies. The cap additionally includes reference and ground electrodes, which can be freely positioned; in the example from Fig. 3, Left Pre-Auricular (LPA) and Right Pre-Auricular (RPA) points from the 10–20 EEG system were used.

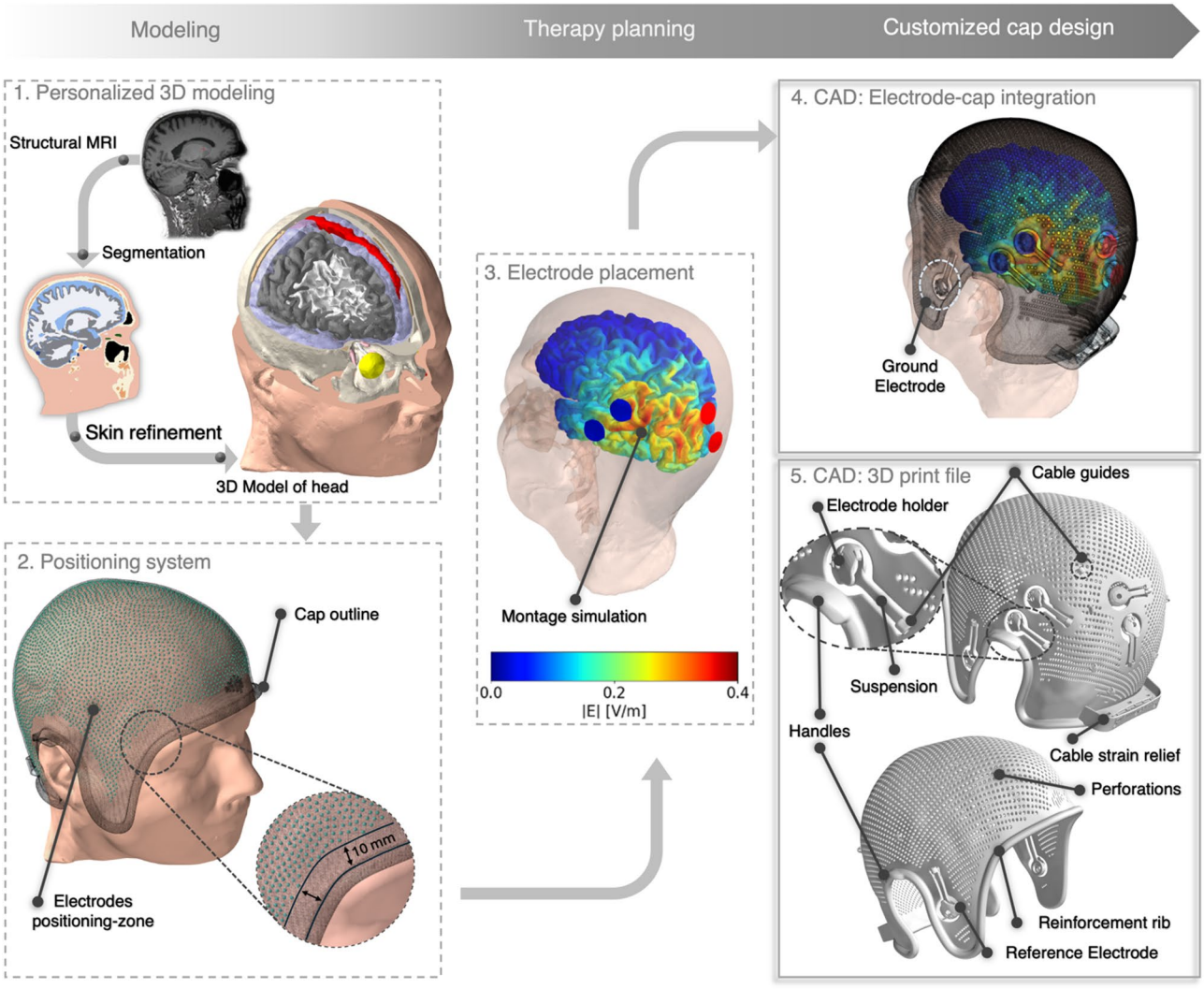

Fig. 3 Full pipeline for designing the customized 3D-printed tES/EEG cap. **(1)** Personalized 3D models are created from each subject's MRI scans via segmentation and meshing. **(2)** The cap outline is created using the skin surface mesh, which then defines a dense grid of available electrode positions. The magnified region shows the 10 mm offset from the cap outline to the grid of electrode positions. **(3)** Electrodes are placed on the cap according to requirements of the treatment and optionally Finite Element Method (FEM) simulations or optimizations. **(4)** The cap is designed with electrode holders based on the proposed montage(s). **(5)** All features of the final customized cap are added to the design, which can then be send for 3D printing

Integrating electrodes into the cap

The electrode positions can be accurately integrated into the cap because their coordinates are given in the same subject space where the cap is generated using CAD. The electrode holders are attached to the cap shell *via* suspended arms that apply a force to ensure proper contact between the electrodes and scalp, which has the additional benefit of enhancing the cap's grip on the head. Electrode suspensions are placed to ensure electrodes sit in the desired position and height above the scalp, then they are oriented to prevent collisions. The arms can be gently wiggled side to side to part the hair and ensure good electrode-scalp contact scalp in hair covered areas without changing their intended positions.

Final cap design

In a final step, additional design features are integrated into the cap. Perforations in the shell are added to enhance ventilation and prevent sweating during therapy. To ensure a secure fit and minimize movement, rigidity in regions such as the frontotemporal, mastoid, and pjarotid-masseteric areas is important. Therefore, a reinforcement rib along the outline of the cap provides structural strength and rigidity. Cable guides are incorporated and cable lengths are calculated to ensure a clean and organized layout with minimal cable length for improved signal to noise ratio during EEG recordings. The cap is connected to the neurostimulator electronics housed in a neckpiece with a cable strain relief system at the posterior section of the cap to prevent cable disconnection

in the case of dramatic movements or a dropped device. Handles are added above the ears to facilitate the user to take the cap on and off.

Multi-step tES/EEG electrode placement

As part of a Miamind® Neurostimulator/EEG device system, the customized cap can accommodate up to 34 electrode positions, including ground and reference channels. The device supports multi-step tES and EEG recordings within a single session, and placement of both stimulation and EEG recording electrodes is flexible. Figure 4 illustrates the process for determining the number and placement of electrodes on the final cap based on the initial therapy prescription. First, the stimulation montage for each tES step is selected. If EEG recording is not required or is limited to the same stimulation electrodes, the pipeline proceeds directly to the CAD design of the cap. However, if additional EEG-only electrodes are needed, these positions are added to the tES electrode positions on the cap, with a maximum of 34 total electrodes (including reference and ground). In the example depicted in Fig. 4, the prescription includes three tES steps, each targeting a separate ROI. For each ROI, an optimization is performed using a dense grid positioning system on a personalized head model applying cap's design constraints. Each optimized montage includes four electrodes, resulting in a total of 12 tES electrodes. Together with the reference and ground electrodes, this results in a customized cap containing 14 electrodes (Cap A). If an EEG recording step with 32 channels is also included in the prescription, an additional 18 EEG electrodes must be integrated into the design. These EEG-only electrodes can be flexibly placed but are typically selected from the standard 10–20 positioning system using an algorithm that ensures uniform coverage of the head. This allows for EEG analysis including microstate extraction and source analysis without gaps in electrode coverage (Cap B). The positions of the reference and ground electrodes can be customized based on the specific needs of the therapy protocol [55].

The full neurostimulator tES/EEG system components

Once the customized neurostimulator cap with up to 34 electrode positions is 3D-printed, the complete Miamind® Neurostimulator/EEG device is assembled. The components of the assembled device are outlined in Fig. 5. The assembly process involves connecting electrode sites to the control electronics housed in the neckpiece *via* the

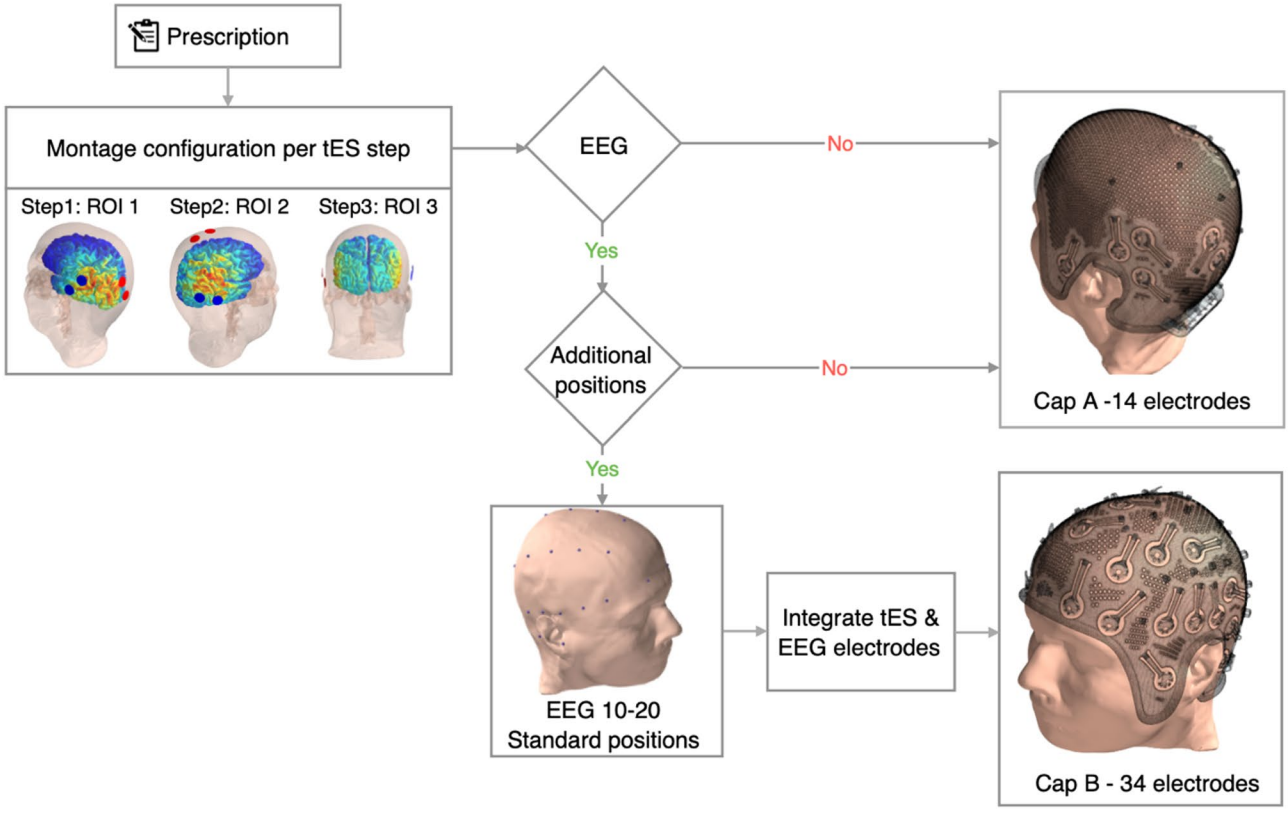

Fig. 4 tES and/or EEG electrode placement. In addition to tES, therapy protocols may feature EEG recordings. In this case, EEG can use electrodes placed for tES and, optionally, additional electrodes. For example, EEG-only electrodes can be placed in custom or standard positions subject to the total number of electrodes not exceeding 34

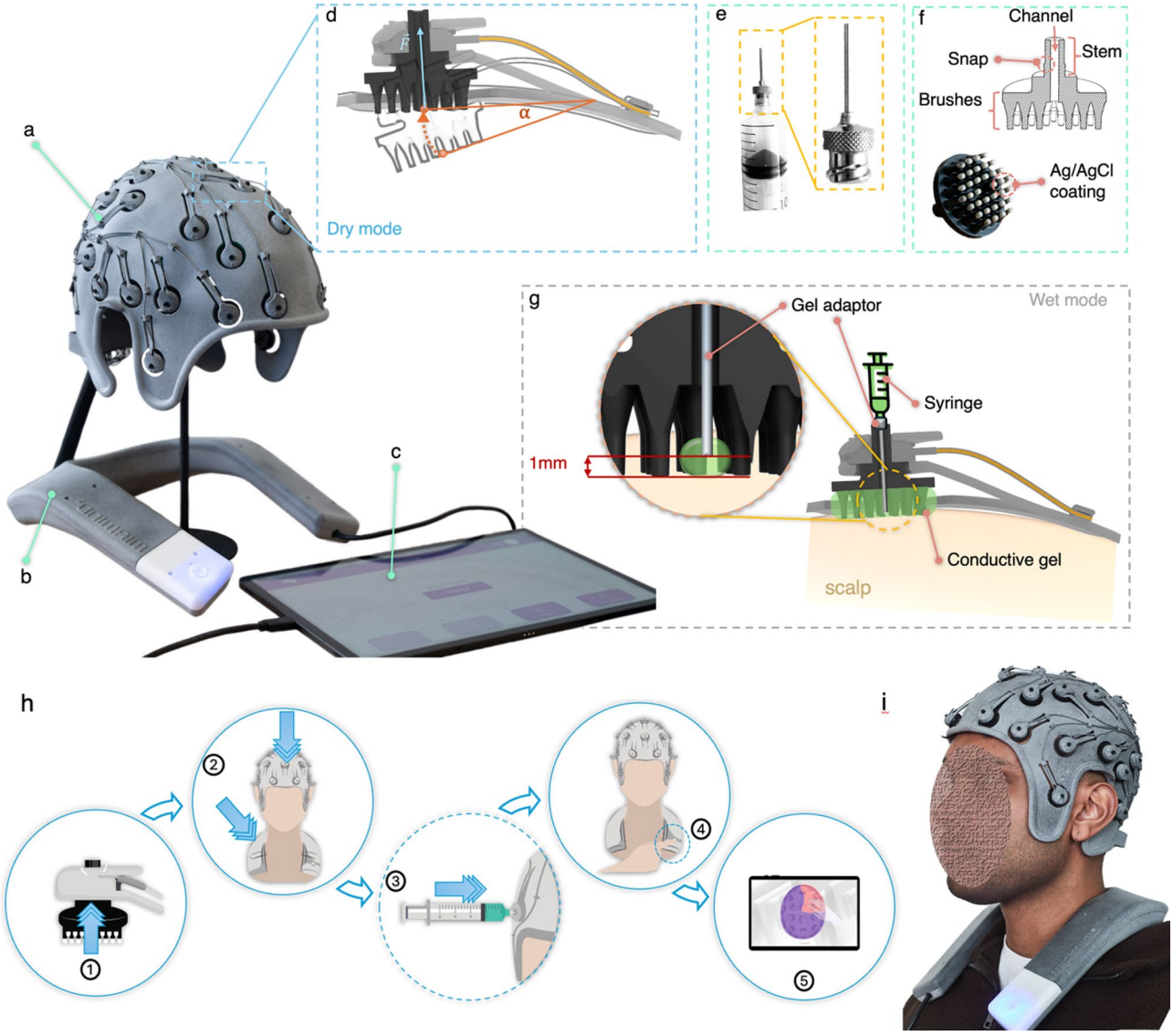

Fig. 5 Components of the custom-made tES Miamind® Neurostimulator/EEG medical device. **a** Customized 3D-printed cap with integrated electrode positions. **b** Neckpiece containing neurostimulator and EEG recording electronics. **c** Tablet with dedicated Android application that serves as the power supply for the system. **d** Electrode suspension holders with inserted brush electrodes; a is the angle between rest and extended states of suspension arm (about 10°). **e** Syringe and gel adaptor for gel injection. **f** Design of the Ag/AgCl-coated brush electrodes for use in both dry and wet mode. **g** Operation in wet mode; conductive gel is injected through the electrode channel and brushes. **h** Miamind® Neurostimulator/EEG device setup workflow. **i** The 3D-printed customized device in use by a subject

integrated cable guides and strain relief system (Fig. 5a). A therapy session is started by pressing a button on the neckpiece (Fig. 5b). While the electrodes are removable for cleaning and replacement, the electrode sites remain connected with a fixed mapping to the control electronics to avoid human error and minimize set-up time. The neckpiece is sealed during assembly and quality control tests are performed to confirm the functionality of the entire device. Neurostimulator devices are delivered with conductive gel, a syringe, and a gel adapter for reducing contact impedance with the scalp if necessary. A tablet serves as the power supply to the whole system and allows patients to monitor the stage of the therapy during a session using a dedicated Android application (Fig. 5c). The tablet also securely uploads EEG data and patient feedback to cloud storage.

Hybrid cap electrode design

The cap-electrode system supports operation in both dry and wet modes, enabled by the combination of suspension arms on the cap and hybrid brush electrodes (Fig. 5). The electrodes snap into the electrode holders with a stem that passes through an opening in the holder. When fixed, the top section of the stem extends approximately

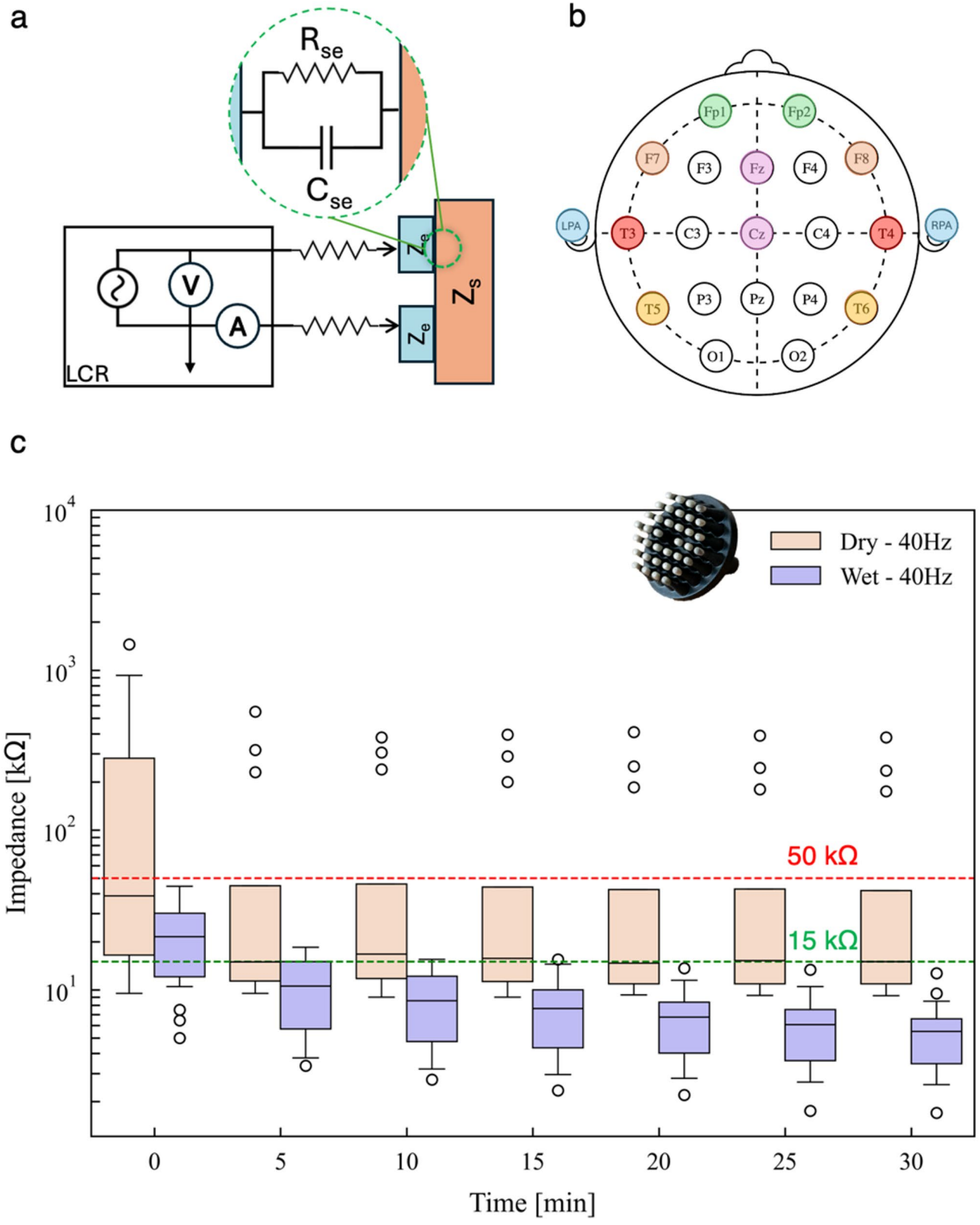

Fig. 6 (See legend on next page.)

(See figure on previous page.)

Fig. 6 Ag/AgCl-coated hybrid brush electrodes can reach mean impedance of 15 k Ω in dry mode. **a** Simplified schematic of skin-electrode interface impedance test setup: Ag/AgCl-coated brush electrodes (blue boxes, impedance Z_e) are placed on scalp (orange box, impedance Z_s). Zoom in: the electrical circuit equivalent for skin-electrode interface impedance (Z_{se}) composed of resistance (R_{se}) and capacitance (C_{se}). **b** Positions of electrode pairs (matching colors) on all subjects' heads for each measurement based on standard EEG positioning system. **c** Boxplots of Z_{se} for all subjects and electrode pairs over time at 40 Hz in dry (orange) and wet (violet) mode, i.e. using conductive gel. Impedances of 15 k Ω (green) and 50 k Ω (red) are indicated with horizontal dashed lines

2 mm above the surface of the holder. A channel in the stem facilitates the injection of conductive gel when necessary.

The electrode features 36 brushes, each 5 mm long, for use on hair-covered regions of the scalp. The thirty-six brushes have approximately 113 mm^2 of surface contact in dry mode when fully in contact with the skin. To enhance conductivity and reduce skin-electrode impedance, the tips of the brushes are coated with Ag/AgCl [56]. In the resting state when the cap is not worn, the suspension arms hold the electrodes at an angle of approximately – 10° relative to the cap surface. When the cap is placed on the head, the electrodes are pushed outward by the scalp, aligning at 0° and applying a consistent force of about 2 N (Fig. 5d). This force can be adjusted by modifying the geometry and thickness of the suspension arms to control their stiffness. The angular alignment and flexible arms ensure the brush electrodes make parallel contact with the scalp, distributing pressure evenly across all brush tips, which enhances comfort while maintaining reliable electrical contact. This pressure increases the surface contact between the brush tips and the scalp thereby reducing impedance, particularly in dry mode.

If the impedance remains high due to factors such as dense hair or specific skin types, conductive gel can be injected through the electrode's stem channel using the gel adaptor and a syringe filled with conductive gel. When inserted to its full length, the adaptor is 1 mm shorter than the electrode to prevent direct contact with the scalp and allow gel to penetrate through the hair to the scalp (Fig. 5g). The tip of the gel adaptor is blunted for safety. Tests showed that in regions with no hair, the empty space between the electrodes and scalp can be filled with 0.8 ± 0.1 ml of gel to cover a surface area of 254 ± 30 mm^2 on the scalp.

Device setup is outlined in Fig. 5H: First, brush electrodes are snapped into the designated electrode holders. Next, the subject places the neckpiece around their neck and fits the cap-electrode system onto their head. To ensure proper contact between the brush electrodes and the scalp, the subject may need to gently push or wiggle the electrodes to allow the brushes to penetrate through the hair. The suspension design allows for slight electrode movement (a few millimeters) without compromising the positional accuracy of the cap. In the optional third step, conductive gel can be injected through the electrode channels. It is particularly useful for ensuring electrode-skin contact in subjects with dense or long hair. Once the cap is positioned, the subject initiates the therapy by clicking the start button on the neckpiece. The system performs an impedance check automatically and indicates which electrodes (if any) need improved contact. If the impedance is within acceptable limits, the therapy begins. If not, the user can lower impedance by either applying a small amount of gel or readjusting certain electrodes by wiggling them, at which point the therapy will start automatically.

Validation of hybrid Ag/AgCl-coated brush electrodes

Hybrid brush electrodes were tested to determine their electrical and mechanical properties as well as the quality of brain signal acquisition. The impedance for Ag/AgCl-coated brush electrodes (Z_e) was 80 ± 10 W in a test setup in contact with highly conductive copper foils (0.95 ± 0.10 W) and remained consistent over frequency range of 20–3000 Hz (Fig. S3). The phase was zero over this frequency range, indicating that the impedance remains dominantly resistive and voltage and current resonant in phase [57].

Figure 6 shows the skin-electrode interface impedance (Z_{se}) measurements for brush electrodes installed on customized caps for five subjects with hair length ranging from 10 up to 50 mm and various hair types and densities. Figure 6a and B illustrate the simplified circuit model of the skin-electrode interface impedance tests and positions of electrode pairs on the subjects' heads using 10–20 standard EEG positioning system, respectively. The Z_{se} (on the order of k Ω) is much higher than the electrode and tissue impedances (on the order of Ω), thus we can consider the measured impedance approximately the sum of Z_{se} for both electrodes in contact with scalp placed in series. As a result, the Z_{se} for one electrode is approximately the half of the value measured on LCR meter. The boxplot in Fig. 6c presents the impedance values for electrodes in both wet and dry modes at frequencies 40 Hz (see Fig. S4A for measurements in frequency of 1 kHz) over time (30 min, divided into 5-minute intervals) for the described test setting. Each box represents distribution of a specific mode at a given time point and frequency. We took the $Z_{se} \leq 15$ k Ω as an indicator for sufficient impedance value for tES application assuming injection of 2 mA total current for two electrodes based on the safety measures [58] by applying maximum voltage of ± 15 V. Over time, there is a general

decrease in impedance in both dry and wet modes across both frequencies, reflecting electrode-skin contact stabilization. The drop is more pronounced for wet electrodes indicating that gel settles on the skin and increases contact area over time. After five minutes, impedance in both conditions stabilize. Dry electrodes exhibit overall higher impedance with mean around 15 kΩ, with some data points towards higher values (above 100 kΩ). Closer inspection at the data points in 40 Hz in Figure S4B, suggests that the inter-subject variability is the primary factor, as indicated by the multi-modal distribution of the datapoints. Prior studies have suggested that this variability may be attributed to differences in skin type rather than hair density or the region of measurement on the subjects' heads [59]. Such statement can be confirmed by another representation of data according to the with and without hair region in Fig. S5. Wet electrodes show consistently lower impedance, particularly at 1 kHz, where the values after minute five are tightly distributed between 1 kΩ and 4 kΩ. This is typical in bioelectrical measurements due to capacitive effects [60, 61]. Note that this experiment has been conducted without any skin preparation such as abrasion or cleaning. Generally, wet mode was below 15 kΩ for all subjects and positions, while dry mode was below 50 kΩ for most subjects and positions.

The performance of brush electrodes in dry mode was compared to standard Ag/AgCl cup electrodes in wet mode using conductive paste for EEG signal acquisition, see Fig. 7. Recordings were conducted simultaneously in both eyes open and eyes closed conditions from frontal positions AF7, Fp1, AF8, and Fp2 on the forehead with both electrode types placed as close as possible (Fig. 7a). Figure 7b presents the power spectral density for both electrode types across different frequency ranges. The brush electrodes in dry mode show a comparable performance to the wet mode cup electrodes, with clear spectral peaks around 10 Hz (alpha frequency band) under both eyes open and eyes closed conditions. The inset shows the EEG signal traces over time, highlighting that the dry brush electrodes capture EEG signals with similar fidelity to the wet cup electrodes, even for subtle eyeblink artifacts. The coherence between electrode pairs at different frequency bands is illustrated in Fig. 7c. Across the delta, theta, alpha, beta, and gamma bands, the brush electrodes in dry mode show comparable coherence values to the wet cup electrodes. The inset further quantifies the signal-to-noise ratio (SNR) before and after filtering for low-frequency noise and 50 Hz electrical interference. Both electrode types have high SNR performance (mean SNR of 0.82 and 0.83 for Miamind electrodes and standard cup electrodes, respectively). Finally, Fig. 7d shows the correlation between the signals recorded from adjacent pairs of electrodes (FP1-AF7 and FP2-AF8) for both electrode types in eyes open and eyes closed conditions. The correlation is high (close to 0.99), indicating nearly identical signals from dry brush and wet cup electrodes. Overall, these results indicate that brush electrodes in dry mode perform comparably to standard Ag/AgCl cup electrodes in wet mode across all key metrics for EEG signal acquisition.

The brush electrodes remained intact with no signs of breakage or peeling of the Ag/AgCl coating during both real-time and accelerated cyclic loading tests, confirming their durability and reusability (Figure S5). Furthermore, they have been deemed biocompatible by passing ISO 10993-5 cytotoxicity tests. The electrodes meet the necessary safety standards for medical use in contact with skin with and without use of conductive gel and are thus certified as a Class I medical device under Swissmedic.

Usability and performance of the miamind® neurostimulator/EEG device

The Miamind® Neurostimulator/EEG device was tested on healthy subjects ($N=8$) as part of the MindStim clinical trial (NCT05999916) to evaluate its safety and performance. The therapy protocol for the MindStim trial is shown Fig. S6. Subjects had four sessions each with three steps of tACS (for three target ROIs) and EEG recordings before and after each tACS step. Each subject received a customized cap with 34 electrodes (2 electrodes were used as reference and ground electrodes), similar to cap B in Fig. 4, and used conductive gel to reduce the impedance, specifically for tACS. All participants completed all the intervention sessions. Also, out of 128 EEG recordings, only two were excluded due to persistent muscle artifacts that could not be removed using independent component analysis (ICA).

In addition to EEG data, participant feedback was collected through a questionnaire after final visit. All respondents felt comfortable during the use of the system and most (7 out of 8) were content how easy the system is to use. 7 out of 8 participants rated the cap and neckpiece design as comfortable. 1 participant reported discomfort of the cap and during stimulation. Willingness to extend stimulation duration was moderate, 5 out of 8 expressed willingness of sessions lasting longer than one hour. All participants found daily clinic sessions manageable, and 7 out of 8 expressed interest in conducting the therapy by themself at home. Importantly, no respondents reported discomfort with the therapy, indicating a positive overall experience with minimal barriers to compliance. Daily usage was generally acceptable if no gel injection is required (7 out of 8). These findings indicate that participants prefer the device for home-based daily use if designed with minimal setup, such as gel-free operation (Table S1). A total of 32 one-hour tACS sessions were conducted using the Miamind® Neurostimulator, with no

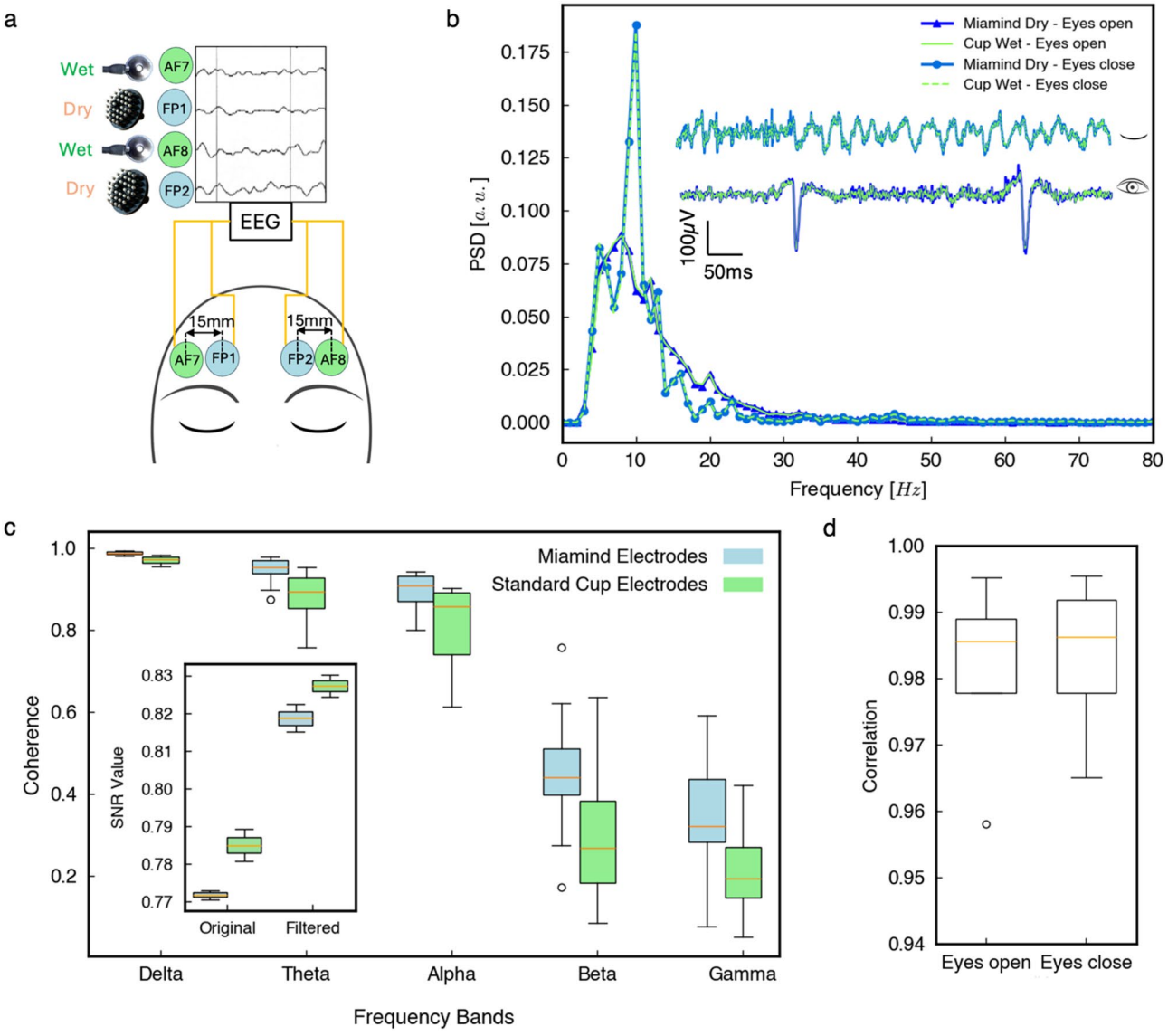

Fig. 7 Ag/AgCl-coated brush electrodes in dry mode match the performance of standard cup electrodes in wet mode for EEG signal acquisition. **a** Schematic of the test setup for EEG recordings of Ag/AgCl-coated brush electrodes in dry mode compared with clinically standard cup electrodes in wet mode. **b** Power spectral density (PSD) for the two electrode types under both eyes open and closed conditions. Inset: overlayed signals in time domain. **c** Coherence between pairs of electrodes of same type for different band frequencies in eyes closed condition. Inset: Signal to noise ratio (SNR) for both electrode types for the original and filtered signals (0.5 to 100 Hz bandpass and 50 Hz notch filters). **d** Correlation of signals between adjacent wet cup and dry brush electrodes (FP1-AF7 and FP2-AF8) for eyes open and closed conditions

Serious Adverse Device Effect (SADE) or Unanticipated SADE (USADE) reported during any of the sessions. None of the participants paused the intervention during any of their 4 sessions.

Table 1 demonstrates a comparison to other available state-of-the-art tES/EEG devices. At present, this device is the only tACS device intended for use at home that is registered as custom made medical device according to Annex XIII EU-MDR in the EU, the United Kingdom, and Switzerland. Unlike conventional systems relying on generic, low-density montages with manual setup, our pipeline combines therapeutic accuracy with unsupervised ease-of-use in a fully integrated solution.

Discussion

In this study we present the development of a novel manufacturing pipeline for clinically viable device for personalized tES therapy and EEG recording, which was informed by the following design requirements: (i) flexible, personalized electrode placement; (ii) repeatable, accurate fit on the patient's head; (iii) ease-of-use to accommodate at-home application; (iv) acceptable contact impedance without extensive head/skin preparation.

Table 1 Comparison of features from available tES/EEG devices[†]

	This device	Ref. 1*	Ref. 2**	Ref. 3***	Ref. 4****
Technology	tDCS, tACS, EEG, custom waveform	tDCS, tACS, EEG, tRNS, custom waveform, TI	tDCS	tDCS	tDCS, tACS, tRNS (4 waveform)
Hardware Specification					
Medical grade	Custom made MD (CH, UK, EU)	Research only	Class IIa MD (EU, UK)	Class IIa MD	Research only
Power supply	Tablet power, rechargeable	Built-in, rechargeable	Built-in, rechargeable	Built-in, rechargeable	Built-in, rechargeable
Number of channels	Up to 32	32	2	2	2
Ground electrode	Build-in, customized position	Ear clip	Collector electrode	N/A	N/A
Electrodes (wet mode)	Ag/AgCl-coated brush electrodes	Ag/AgCl disk electrodes Sponge electrodes Kendall™ H124SG electrodes	Sponge electrodes	Rubber electrodes with sponge pads (rectangular and circular and ring shapes)	Rubber electrodes with sponge pads (rectangular and circular and ring shapes)
Electrodes (Dry mode)	Ag/AgCl-coated brush electrodes (36 points over area of 2 cm^2)	Ag/AgCl Drytrode (10 points over area of 1.3 cm^2)	None	None	None
Communication	Wireless (SIM card)	Wireless	Bluetooth controlled through app	USB port to a PC with internet connection	USB port to a PC with internet connection
PCB house	Neckpiece	box on back of cap	Build-in headset	Portable Hardshell case	Portable Hardshell case
EEG recording	Yes	Yes	No	No	No
Electrode holders Specification					
Technology	3D-printed rigid cap	Fabric cap	Headset	Fabric cap	Fabric cap
Material	PA12 (USP class VI, FDA certificate)	Neoprene	N/A	Lycra	Lycra
Positions	Flexible on entire electrode positioning zone	Fixed holes based on EEG standard systems (32 or 69 positions)	FP1, FP2 on frontal lobe	Five pairs of positions in frontal and prefrontal regions	Five pairs of positions in frontal and prefrontal regions
Size	Personalized head fit	Four sizes	Adjustable fit	Five sizes	Five sizes
Grip	Patient head morphology	Chin strap	Extended arm to back of head	Chin strap	Chin strap

[†] All information was gathered from original specification sheets of each device and is valid only for the specified product

*Ref. 1: Starstim Neuroelectric,

**Ref. 2: Flow, Flow Neuroscience

***Ref. 3: DC-stimulator mobile, Neurocare

****Ref. 4: DC-stimulator plus, Neurocare

Our in-silico experiments (Fig. 1) showed that compared with fixed HD montages, montages optimized with personalized head models achieved a biologically effective dose in the ROI [21], reduced variability across subjects, and did not substantially sacrifice accuracy or focality. These results are in good agreement with prior studies [14, 16] and increasing flexibility in electrode placement will likely provide further gains. Our recent findings further support this direction, demonstrating that increasing the number of candidate electrode positions from 32 to 86 significantly improved target engagement and reduced off-target field exposure across a variety of stimulation scenarios [62]. In conventional systems, deploying such dense arrays may be impractical due to increased complexity in setup and patient discomfort. However, within our pipeline, there are no major technical or ergonomic drawbacks to higher-density montages. Since electrode placement is digitally optimized and embedded directly into the 3D-printed cap design, the patient receives a fully configured device that requires no manual setup. The CAD model enforces safety constraints, such as minimum spacing to prevent short circuits, while providing maximal flexibility in positioning. Thus, the use of a denser electrode grid in this context allows for improved focality and dosage control without compromising ease of use or comfort. However, practical constraints dictate that many devices still employ non-personalized fixed montages or limit the number of available electrode positions for optimization. Given that variability in tES response is linked to variability in

applied dose [63, 64], next-generation devices must solve this personalization challenge for clinical application. This informs our 3D-printing-based approach, where each cap is customized to an individual.

Simulations mimicking the effects of inconsistent cap placement during real-world usage identified the strong impacts of montage movements due to slight rotational displacements of a cap (Fig. 2). Displaced montages resulted in altered electric field strength and direction in the target ROI, thereby generally reducing on-target and increasing off-target stimulating. This effect is especially critical when specific electric field orientations relative to cortical gray matter are desired [12]. The off-target dosage may also reduce therapy efficacy, particularly if functional networks anti-correlated to the target network are stimulated. This may result due to spatial proximity of anti-correlated cortical nodes, e.g. BA39 (task-negative network) and BA7/40 (task-positive network) [28]. Thus, the efficacy of tES therapy will likely depend heavily on the precise and consistent application of the prescribed montage over many sessions. Accurate replication of montage positions across sessions remains challenging with one-size-fits-all caps that must accommodate varying head shapes and sizes. It is important to note that improved mean $|\vec{E}|$ in ROI, along with its correlation with the ROI due to displacement in certain cases, may be attributed to the constraints of the 82-electrode positioning system used for optimization. This observation underscores the potential benefits of employing denser electrode grids to achieve a more optimized montage. While the rigid rotational model used in this study is primarily applicable to rigid caps, future research should evaluate displacements for elastic fabric caps in real-world application. Our cap design approach seeks to reduce inconsistent cap placement through a rigid cap whose shape is given by the scalp profile extracted from an individual's MRI. To assess inter-session and inter-user variability in cap placement, self-administered electrode placement with the Miamind® neurostimulator/EEG device should be compared to placements by medical professionals using anatomical landmarks. Further studies could explore the use of motion detectors to identify and correct any potential cap mispositioning during use.

In this work we present a pipeline to fabricate a device for personalized therapy that can be precisely set up with minimal effort. Here we integrate structural MRI-based head morphology extraction for customized cap profile and personalized montage selection. The tailored, rigid cap is 3D-printed, ensuring accurate digital-to-physical translation via CAD modeling. A key advantage of this approach is the alignment of CAD coordinate system with the patient-specific 3D head model enabling montage configurations to be directly embedded into the cap design. This integration ensures accurate electrode placement while additional design features enhance grip, rigidity, and ventilation, improving comfort and usability. The cap is designed to fit in only one orientation and reduce the potential for electrode displacement, though future studies should systematically benchmark movements across different head geometry. Ensuring the accurate replication of montage geometries by the real-world users reduces the mismatch between simulated and applied electric field distributions, however these cannot be completely eliminated due to the inherent simplifications and assumptions used in computational models [65].

One of the target clinical indications for this system is Alzheimer's disease, for which structural MRI is typically part of the routine diagnostic pathway. In such cases, the MRI data can be directly integrated into our pipeline for personalized cap design and electrode placement. However, for other conditions, such as depression, structural MRI may not be routinely acquired. In those cases, additional imaging may be required to enable customization. For individuals unable to undergo MRI due to contraindications, alternative approaches can be employed to approximate personalization. For example, a 3D optical scan of the head can be performed while the subject wears a tight-fitting fabric cap to suppress hair volume, allowing for extraction of the scalp surface and configuration of standard electrode positioning systems. While this method does not allow for the generation of personalized internal anatomical models, available brain and head atlases can be utilized to perform simulations and optimizations using these standardized electrode layouts. Despite a reduction in anatomical accuracy compared to MRI-derived models [62], the customized fit of the cap based on individual head surface geometry still offers several advantages over conventional, one-size-fits-all systems, particularly in facilitating improved comfort and repeatability for at-home use. Future work should investigate how 3D photogrammetry-based fitting of normative atlases combined with customized electrode placement could improve electric field distributions.

Hybrid dry/wet Ag/AgCl-coated brush electrodes were designed for the neurostimulator device in both EEG and tES applications. The brush structures extend through hair to contact the skin in areas with short to moderate hair coverage, achieving dry-mode impedance below 15 kΩ for some subjects. However, variable interface impedance between subjects, which is influenced primarily by skin type rather than hair density, necessitates gel injection in certain scenarios. Dry brush electrodes, while advantageous for ease of use, may leave temporary scalp imprints after prolonged sessions; however, these marks typically fade within minutes of removing the headset. The applied contact force is carefully calibrated to remain

within a low range (below 2 N), a contact force well tolerated by users (Table S1), striking a balance between signal integrity and user comfort. The individualized CAD design of the cap allows for further pressure tuning by altering the thickness and angle of the electrode arms based on scalp region, providing softer contact in hairless zones (e.g., forehead) and slightly firmer contact in areas with dense hair. This customization not only ensures reliable scalp contact but also contributes to improved cap stability during movement. For extended therapy sessions where lower impedance and enhanced stability are required, the hybrid electrodes can alternatively be operated in wet mode, which provides additional performance benefits. Selection of dry or wet mode operation can be made by users in real-time based on impedance measurements communicated to the user through the tablet. For tES, wet mode is more suitable because the overall impedance is reduced, thus reducing the applied voltage and resulting sensations under the electrodes. Further investigations are needed to evaluate long-term electrode-skin contact stability in dry mode under varying conditions, including head movement and extended use, particularly for tES applications.

Our findings demonstrate the comparable performance of dry brush electrodes (without skin preparation) and conventional wet clinical electrodes (with skin preparation) for EEG recording in forehead regions. Within the MindStim study (NCT05999916), 2 out of 128 EEG recordings (in wet mode) were excluded for power spectral analysis and EEG biomarker estimation such as vigilance analysis, frontal alpha asymmetry and alpha peak frequency due to excessive muscle artifacts that could not be removed using ICA. Furthermore, the willingness of participants to use the system for extended periods, combined with the lack of serious complaints regarding electrode imprints, supports the overall comfort and usability of the device in prolonged sessions. These results emphasize the potential of the custom cap-electrode system as a reliable and user-friendly solution for simultaneous or separate EEG and tES applications. The integration of flexible electrode placement allows for a range of configurations to adapt to clinical needs, from optimized high-density montages to standard EEG setups. Accurate electrode localization in MRI space also facilitate advanced EEG analyses such as source imaging [66] without restrictions imposed by rough estimation of positions using standard fixed EEG systems [67, 68]. Future research should investigate the impact of asymmetric configurations on source reconstruction quality and electrode distribution strategies in customized tES/EEG systems. The custom made integrated tES/EEG device is ideally suited for advanced tES/EEG synergies, such as closed loop tACS informed by real-time EEG feedback.

The connected tablet serves as both a power supply and a monitoring device for the patients to check impedance and track therapy session progress. This digital interface could also support remote physician assessments and therapy adjustment to reduce the need for frequent clinic visits. Such features could enhance convenience for patients undergoing extended therapy sessions, which can require daily session for up to one-hour over weeks or months.

The system, comprising the cap-electrode interface and the Miamind® Neurostimulator/EEG device, was successfully achieved 100% intervention completion rate in the MindStim safety study (NCT05999916). These results confirm the system's stability, usability, and reliability in an in-clinic setup. However, further validation is necessary to assess suitability in at-home settings under repetitive use over extended periods. Controlled studies should evaluate the feasibility of gel injection, cap fit across various age groups and head shapes, and the performance of the device in diverse real-world scenarios. Importantly, the usability of the Miamind® neurostimulator should be evaluated in clinical populations, as sensitivity to the intervention and perceptions of the device and its performance may vary depending on the user's health status. Symptoms such as altered pain sensitivity, confusion and sensory overload are commonly described due to neurological conditions and might impact the user experience and feedback.

Some limitations on current pipeline should be acknowledged. The primary challenges for personalization of therapy using simulations and comfort of the customized cap are the quality of real-world MRI data and the accurate segmentation of such images, as motion artifacts or spatial distortions can lead to poor model fitting. Moreover, current atlas-based segmentation methods [13, 69] may underperform for heterogenous MRI data or head shapes deviating from standard references, the latter is relevant as tES therapy may target populations with anatomical variations due to aging or disease progression [70]. Currently, manual quality control and segmentation correction are used to mitigate this sort of errors. This could be addressed by integrating deep-learning-based segmentation algorithms designed around heterogenous clinical data [71] into modeling and montage optimization pipelines and ultimately increase the accuracy of cap design, montage configuration and scalability for larger populations. Additionally, electrode placement is constrained by the need to prevent collisions, requiring predefined design constraints in the positioning system and optimization algorithm. As a result, current optimization methods operate within fixed electrode positions [16], limiting their flexibility in determining the most effective montage configurations. These restrictions may reduce the full potential of personalized setups by excluding

viable electrode placements that fall outside the predefined range. Future advancements should prioritize the development of adaptive algorithms capable of dynamically optimizing electrode positioning while adhering to parametric design constraints. Such improvements would enable greater precision in targeting brain regions, leading to enhanced therapeutic efficacy in tES applications. Finaly, while personalization is a major strength, it may be less cost-effective for short-term use cases, such as clinical trials or exploratory research, where stimulation parameters may need to remain flexible and a separate device must be produced per subject.

Overall, this study demonstrates a significant step forward in personalized neuromodulation therapy by integrating computational modeling, 3D printing and hybrid electrode technology. The developed system enables reliable, repeatable, and patient-specific tES and EEG applications, reducing setup complexity by eliminating skin preparation, positioning and fixation, enhancing accessibility for at-home therapy. Furthermore, parametric design enables adaptability for future hardware updates and additional customization. Moreover, recent studies have demonstrating the feasibility and safety of combining non-invasive TI stimulation with intracranial monitoring electrodes [72, 73], highlighting promising directions for the future integration of personalized non-invasive tES with invasive neuromodulation therapies. Future efforts should focus on long-term assessments in clinical populations, integration with adaptive neuromodulation strategies, and further refinement of electrode designs to maximize comfort and efficacy. These advancements will be crucial in transitioning from research-based neurostimulation approaches to widely adopted clinical and home-use solutions.

Methods

Customized CAD design and manufacturing

A software pipeline was developed to facilitate the design and production of customized electrode caps, utilizing a command line interface built with bash scripting and Python 3.9. This pipeline integrated SimNIBS (version 4.0.1) and FreeSurfer (version 7.4.1) to aid in head modelling and montage selection. Personalized head models were used to define a subject-specific coordinate system for cap design, locate fiducials, generate homogeneously distributed dense grid of points on the skin surface, and simulate electric field distributions for montage selection. Once the scalp morphology is modeled and locations of cap electrodes are defined, the digital design of the cap is done in Autodesk® Fusion 360™. Following this, a Rhinoceros® (V7)-Grasshopper pipeline is employed to position all features including electrode placement on scalp within a coordinate system that is aligned with original 3D model. The final mesh shell outline is then defined. Electrode Suspension arms are oriented to prevent collisions and ensure a logical cable routing. Semi-automatic generation of cable guides follow, after which all features are combined to create the final geometry. If quality control tests of the design pass, the final CAD file is sent for print and cable length recommendations are exported to guide assembly.

3D printing of personalized caps

The custom-designed caps were 3D printed at Prodartis AG (Appenzell, Switzerland) using Multi Jet Fusion (MJF) technology on an HP Jet Fusion 5000 3D Printer (HP Schweiz GmbH, Wallisellen, Switzerland). Polyamide 12 (Nylon), certified under FDA food contact regulations and USP Class VI standards, was used as the printing material. This material was selected for its durability and safety for skin contact, making it suitable for prolonged use in neurostimulation applications.

Neurostimulator/EEG device

The Miamind® Neurostimulator tES/EEG device (v1.0.0, REF 00600) was developed by Bottneuro AG (Basel, Switzerland). The device supports a maximum of eight active electrodes per stimulation steps out of up to 34 positions and up to 33 EEG recording channel. It can deliver both DC and AC currents across a frequency range of 20 to 80 Hz. It allows customizable waveform and phase shifts, with adherence to international safety standards including IEC 60601-1:2005 + A1:2012 + A2:2020. The neurostimulator and all materials used in the cap and electrodes underwent biocompatibility and safety testing, meeting the electromagnetic disturbance standards (EN 60601-1-2:2014 + A1:2020, IEC 60601-1-2:2014 + AMD1:2020).

Electrodes

The Miamind® brush electrodes used for EEG and tES were developed by Bottneuro AG (Basel, Switzerland) and registered as Class I medical device according to Swiss agency for therapeutic products, Swissmedic, Switzerland. These electrodes are made from a conductive carbon-rubber material and manufactured using an injection molding method by Dätwyler Holding Inc. (Altdorf, Switzerland). The tips of the brush electrodes are coated with Ag/AgCl.

Gel adaptor

Gel adaptor is developed by Bottneuro AG (Basel, Switzerland) and is a 304 stainless steel needle (18 gauge / blunt needle point) manufactured by Hamilton Central Europe (Timișoara, Romania). The 15 mm length of needles are compatible with Luer lock syringes.

Electrode impedance measurement

For the impedance measurement of the brush electrodes, a copper tape was fixed to a rigid plate with two folded sections of the tape providing contact points for alligator connectors attached to the precision LCR meter (KEYSIGHT E4980AL, Keysight Technologies, CA, United states). Initially, the impedance of the copper plate was measured across a frequency range of 20 Hz to 3 kHz as a normalized value, with both alligator connectors gripping the copper tape. The impedance of the electrodes was then measured by connecting one alligator clip to the electrode's stem while ensuring that all the brushes of the electrode were in full contact with the copper tape under a fixed force of 5 ± 0.5 N, applied using a digital force gauge (EXTECH, model 475040, Teledyne FLIR LLC, Wilsonville, United states). The process was repeated for five randomly selected electrodes from a batch of 400. The impedance of the copper foil ($0.95 \pm 0.10\ \Omega$) was 80 times lower than that of the electrode, confirming its negligible influence on the measurement.

Skin-electrode interface impedance test

The skin-electrode interface impedance for the brush electrodes was assessed on five subjects with varying hair densities. The test was performed on five different pairs of scalp positions that covered all lobes of the head, with measurements taken every five minutes for a total duration of 30 min. Both wet and dry modes were tested, with the wet mode employing a conductive gel (Signa gel Electrode Gel, Parker Laboratories, Inc., Fairfield, USA) without any prior skin preparation. The volunteers, who had short hair (4 ± 2 cm), were required to shower a few hours before the test to ensure consistency in skin conditions. Impedance measurements were performed using a precision LCR meter (KEYSIGHT E4980AL) with a 1 V applied voltage. The electrodes were mounted on a customized 3D-printed cap described in this work, which were designed specifically to ensure consistent electrode positioning and force on the scalp.

EEG signal validation

The validation of the brush electrodes in dry mode for EEG signal acquisition was conducted using an OpenBCI Cyton board (OpenBCI, Brooklyn, NY, united states), an 8-channel EEG acquisition device. The validation procedure involved recording EEG signals for a subject during two sessions, each lasting 3 min, with the subject's eyes open and closed. These sessions were separated by a 1-hour interval. The electrode positions FP1/AF1 and FP2/AF2 were chosen on the non-hair region of the forehead, minimizing the distance between the electrodes (FP1 and FP2) and cup electrodes (AF1 and AF2) with 15 mm distance. For optimal comparison, only the skin region under the cup electrodes was prepared according to clinical standards by cleaning and abrading the skin using Nuprep gel (Weaver and Company, Aurora, USA), and the cup electrodes (reusable 10 mm Ag/AgCl-coated electrodes) affixed with Elefix Z-401CE conductive adhesive paste (Nihon Kohden Corporation, Tokyo, Japan). The brush electrodes were carefully placed on the subject's head without any skin preparation and in dry mode, using a personalized cap while ensuring the cup electrodes remained undisturbed. The recorded EEG signals were processed by applying high-pass and low-pass filters with a cutoff frequency of 0.5 and 100 Hz respectively, along with a notch filter in the 47–53 Hz range to remove noise. The sampling rate for the recordings was set at 250 Hz.

Mechanical characterization

Mechanical testing of the electrodes was conducted using a BOSE ElectroForce 3300 (TA Instruments, New Castle, USA) machine under both real-time and accelerated conditions. Eight brush electrodes were mounted on a polytetrafluoroethylene (Teflon) platform installed on the machine's arm. To simulate the conditions of a human scalp, a stiff flat plate covered with a soft wipe was used as the substrate. In the real-time test, 30 loading cycles were applied each over a 30-minute period, with a force of up to 1.5 N per electrode. For the accelerated simulation, 500 loading cycles were performed with a force of up to 3 N per electrode. This mechanical characterization aimed to evaluate the durability of the electrodes under conditions replicating both short-term and long-term use.

Clinical trial

The MindStim clinical trial (NCT05999916) was an exploratory, first-in-human, single-arm, monocentric study aimed at evaluating the safety and tolerability of tACS delivered by the Miamind® Neurostimulator/EEG device in healthy participants. The trial involved ten participants who provided informed consent for the use of their MRI scans. Eight participants underwent the full study protocol. The study was approved by the Independent Competent Ethics Committee Ethikkommission Nordwest-und Zentralschweiz and Competent Regulatory Authority Swissmedic (BASEC No: 2023-D0054).

Each participant attended four interventional sessions, each included 60 min tACS over four consecutive days. The stimulation frequency was 40 Hz, with a maximum current of 1 mA per electrode and 2 mA total across all active electrodes. The stimulation targeted the left angular gyrus, right angular gyrus, and bilateral temporal lobes, based on individual MRIs, with each region stimulated for 20 min with EEG recordings before, after and in between the tACS steps shown in Fig. S7. Usability of the Miamind® neurostimulator was assessed through

participant feedback questionnaire after the final intervention. To minimize potential response bias, participants completed the questionnaires independently using a digital format. The questionnaire covered six domains: General Impression, Cap and Neckpiece, Application and Tablet, Electrodes of the Cap, Therapy Experience, and Use Outside of the Clinic. Responses were recorded using a 6-point Likert-type scale: Fully agree, Mostly agree, Undecided, Mostly disagree, Fully disagree, and Irrelevant/No answer, and were analysed using descriptive statistics (e.g. frequency counts and percentages) (Table S1).

EEG data preprocessing was conducted using a standardized pipeline to ensure high-quality signal extraction across all sessions by independent experts at Deeppsy (Zürich, Switzland). To minimize noise, eyes-closed (EC) segments were analyzed. For further processing, raw data was cropped into segments. Then, a finite impulse response (FIR) bandpass filter was applied with cut-off frequencies of 0.1 Hz and 70 Hz to retain the relevant physiological EEG signals while removing slow drifts and high-frequency noise. Additionally, a 50 Hz notch filter was applied to remove power line interference. To minimize spectral leakage, data were processed with Hanning window. Electrooculogram (EOG) signals were derived by subtracting F7 and F8 channels to aid in detecting ocular artifacts. Broken channels were visually inspected and interpolated using spline interpolation. Technical and muscular artefacts were marked and artefact correction using ICA was performed. Remaining artefacts were visually inspected to identify high frequency noise due to muscular activity, eyes movements and blinks and environmental noise (i.e., electric peak or wire oscillations). A total of 2 out of 128 EEG recordings were removed due to excessive muscle artefacts.

MRI acquisition and personalized head modeling

High-resolution isotropic T1- and T2-weighted MRI scans ($1 \times 1 \times 1$ mm^2) were acquired for all participants using a Siemens Prisma 3T scanner (Siemens Healthcare, Erlangen, Germany) at the University Hospital of Basel. The field-of-view included the entire head, from cranial skin to the C3 vertebra, with minimal head constraints to reduce skin deformation. Personalized 3D head models were generated using SimNIBS' CHARM (version 4.0.1) software [13, 16. failure in CHARM's automatic segmentation was semi-automatically corrected. Mesh reconstruction and surface smoothing were applied to the final segmented volumes using CHARM to produce accurate 3D models for each subject [74].

In-silico experiments

Simulation experiments were performed using head models of ten healthy subjects enrolled in the MindStim trial who signed the informed consent for the use of their MRI data. The anatomical ROIs were identified using FreeSurfer's recon-all (version 7.4.1) [75] brain parcellation, specifically targeting the left angular gyrus as defined by the Destrieux atlas parcellation (tag 11125, "ctx_lh_G_pariet_inf-Angular"). The stimulation montage involved electrodes of 18 mm in diameter. Simulations were conducted using SimNIBS (version 4.0.1) [76], with fixed 4:1 HD electrode positions generated by the CHARM routine [74] placed at P3 (+ 2 mA) and CP3, P1, P5, and PO3 (-0.5 mA each). The optimization performed on same subjects, targeted an intensity of 0.3 V/m within the ROI with maximum current per electrode of 2 mA and maximum total current of 4 mA. For optimization of montage for each subject, custom dense grid positioning system with average total number of 86 positions within the electrode positioning zone of customized cap has been used.

Montage displacement experiments were performed for one selected subject with a montage optimized for left angular gyrus as a basis. Simulations were conducted by systematically displacing the entire montage via rigid rotations covering a grid of 125 points, covering – 10° to 10° rotations about all three axes (x, y, z) with 5° intervals over 5 steps. The origin for rotation was taken to be the 0,0,0 point using world coordinates in subject space. After rotation, electrode positions were projected onto the scalp and the resulting montage was simulated.

Statistical analysis

For In-silico study, simulated electric fields from all montages were interpolated onto the central gray matter surface for each subject. Visual assessment was based on renderings generated with PyVista version 0.41.1 [77]. Two quantitative metrics were considered: the mean electric field magnitude in ROI, and the correlation of the electric field magnitude with the ROI to capture the conformity of the field magnitude to the target. The equality of variances is reported with Leven's test with P value indicated in the Figure legend. Experimental data such as Impedance data and EEG signals were further analyzed through custom python version 3.11.0 scripts and visualized through matplotlib version 3.9.0 and seaborn version 0.13.1 [78] toolboxes. For the MindStim study, Data cleaning and analysis were conducted using R version 4.4.0 (The R Foundation for Statistical Computing Platform, 2024). R Studio version 2024.04.2, Build 764 (Posit Software, PBC, 2009–2024), served as the graphical user interface for R. The software applications were installed on Windows 11 Home 23H2 (OS Build 22631.4112). Descriptive statistics were employed to present the device safety and functionality assessed by multiple experience questionnaires. All adverse events recorded throughout the study were categorized and summarized descriptively

by type, severity, and relationship to the device/procedure. Categorical variables (both ordinal and nominal) were summarized using counts and percentages within each category. For numeric variables (continuous and discrete), the descriptive statistics included the number of observations, mean, median, standard deviation (SD), and quartiles (Q1 – Q3), where applicable.

Supplementary Information

The online version contains supplementary material available at https://doi.org/10.1186/s12984-025-01769-8.

Supplementary Material 1

Acknowledgements
We thank the team at the University Hospital in Basel for their contribution in MindStim clinical trial.

Author contributions
Conceptualization: MJ, AH, ES, BO; Methodology: MJ, GR, AH, MRK, RG, MM, BO; Software: MJ, GR, MRK, JSV, JF; Validation: MJ, GR, AH, RG, JSV, JF, MF; Formal Analysis: MJ, GR; Investigation: MJ, GR, AH, RG, AR; Resources: MJ, AH, RG,; Data Curation: MJ; Writing – Original Draft Preparation: MJ; Writing – Review & Editing: MJ, GR, AH, ES, BO; Visualization: MJ; Supervision: MJ, AH, RG, BO; Project Administration: MJ, AH, RG, BO; Funding Acquisition: AH, MM, BO.

Funding
This work was funded by: Bottneuro AG and Innosuisse - Swiss Innovation Agency, Project title "Personalized, 3D-printed brain recording and stimulation headset with integrated conductive tracks", start date 01.04.2023, end date 31.03.2026, project number 102.809 IP-ENG.

Data availability
Availability of MRI Data is restricted due to legal and ethical reasons. Access to MRI data is solely granted if data protection is guaranteed. Availability of Analysis codes is restricted due to the commercial nature of Bottneuro AG. Access to all data and code is subject to approval and a data sharing agreement between Bottneuro and the third-party. Requests to access the data should be directed to Bottneuro AG (www.bottneuro.ch, contact: [mail@bottneuro.ch](mailto: mail@bottneuro.ch))

Declarations

Ethics approval and consent to participate
The study was approved by the Independent Competent Ethics Committee (Ethikkommission Nordwest-und Zentralschweiz (EKNZ)) by the 14 August 2023 and Competent Regulatory Authority Swissmedic by the 20 December 2023 (BASEC No: 2023-D0054). All participants provided their written informed consent to participate in the study before the participant was enrolled in the study and subjected to any investigation-related procedure. The investigation was carried out in accordance to the approved protocol and its amendments, the World Medical Association Declaration of Helsinki (64th WMA General Assembly, Fortaleza, Brazil, October 2013) and Swiss law.

Consent for publication
Not applicable.

Competing interests
M.J., G.R., A.H., M.R.K., R.G., A.R., M.F. and B.O. receive monetary and/or equity or stock from Bottneuro AG. B.O. is a board member of Bottneuro AG. M.J. and B.O. are coinventors on two patents #EP4204077B1 and #EP4282464B1 issued to Bottneuro AG. R.G and E.S., has consulting and/or advisory agreement with Bottneuro AG. The other authors declare that they have no competing interests.

Author details
[1]Bottneuro AG, Basel, Switzerland
[2]Department of Biomedical Engineering, University of Basel, Allschwil, Switzerland
[3]Department of Neurosurgery, University Hospital and University Children's Hospital Basel, Basel, Switzerland
[4]Precision Neuroscience and Neuromodulation Program, Gordon Center for Medical Imaging, Massachusetts General Hospital, Harvard Medical School, Boston, USA
[5]Department of Neurology and Radiology, Massachusetts General Hospital, Boston, USA
[6]Product Development Group Zurich pd|z, ETH Zürich, Zurich, Switzerland
[7]inspire AG, Product Development Group Zurich pd|z, Zurich, Switzerland

Received: 19 March 2025 / Accepted: 4 October 2025
Published online: 24 November 2025

References

1. Grover S, Nguyen JA, Viswanathan V, Reinhart RM. G. High-frequency neuromodulation improves obsessive–compulsive behavior. Nat Med. 2021;27:232–8.
2. Yavari F, Jamil A, Mosayebi Samani M, Vidor LP, Nitsche MA. Basic and functional effects of transcranial electrical stimulation (tES)—An introduction. Neurosci Biobehavioral Reviews. 2018;85:81–92.
3. Reed T, Cohen Kadosh R. Transcranial electrical stimulation (tES) mechanisms and its effects on cortical excitability and connectivity. J Inherit Metab Dis. 2018;41:1123–30.
4. Woodham RD, et al. Home-based transcranial direct current stimulation treatment for major depressive disorder: a fully remote phase 2 randomized sham-controlled trial. Nat Med. 2024;1–9. https://doi.org/10.1038/s41591-024-03305-y.
5. Grover S, Fayzullina R, Bullard BM, Levina V, Reinhart R. M. G. A meta-analysis suggests that tACS improves cognition in healthy, aging, and psychiatric populations. Sci Transl Med. 2023;15:eabo2044.
6. Elyamany O, Leicht G, Herrmann CS, Mulert C. Transcranial alternating current stimulation (tACS): from basic mechanisms towards first applications in psychiatry. Eur Arch Psychiatry Clin Neurosci. 2021;271:135–56.
7. Wischnewski M, Alekseichuk I, Opitz A. Neurocognitive, physiological, and biophysical effects of transcranial alternating current stimulation. Trends Cogn Sci. 2023;27:189–205.
8. Bréchet L et al. Patient-Tailored, Home-Based Non-invasive brain stimulation for memory deficits in dementia due to alzheimer's disease. Front Neurol 12, (2021).
9. De Paolis ML, et al. Transcranial alternating current stimulation (tACS) at gamma frequency: an up-and-coming tool to modify the progression of alzheimer's disease. Transl Neurodegener. 2024;13:33.
10. Da X et al. Noninvasive gamma sensory stimulation May reduce white matter and Myelin loss in alzheimer's disease. Journal Alzheimer's Disease Preprint, 1–14 (2023).
11. Beliaeva V, Savvateev I, Zerbi V, Polania R. Toward integrative approaches to study the causal role of neural oscillations via transcranial electrical stimulation. Nat Commun. 2021;12:2243.
12. Liu A, et al. Immediate neurophysiological effects of transcranial electrical stimulation. Nat Commun. 2018;9:5092.
13. Puonti O, et al. Accurate and robust whole-head segmentation from magnetic resonance images for individualized head modeling. NeuroImage. 2020;219:117044.
14. Dmochowski JP, Datta A, Bikson M, Su Y, Parra LC. Optimized multi-electrode stimulation increases focality and intensity at target. J Neural Eng. 2011;8:046011.
15. Saturnino GB, Madsen KH, Thielscher A. Optimizing the electric field strength in multiple targets for multichannel transcranial electric stimulation. J Neural Eng. 2021;18:014001.
16. Saturnino GB, Siebner HR, Thielscher A, Madsen KH. Accessibility of cortical regions to focal TES: dependence on Spatial position, safety, and practical constraints. NeuroImage. 2019;203:116183.
17. Violante IR, et al. Non-invasive Temporal interference electrical stimulation of the human hippocampus. Nat Neurosci. 2023;26:1994–2004.
18. Grossman N, et al. Noninvasive deep brain stimulation via temporally interfering electric fields. Cell. 2017;169:1029–e104116.

19. Beanato E, et al. Noninvasive modulation of the hippocampal-entorhinal complex during Spatial navigation in humans. Sci Adv. 2024;10:eado4103.
20. Soleimani G, Kupliki R, Paulus M, Ekhtiari H. Dose-response in modulating brain function with transcranial direct current stimulation: from local to network levels. PLoS Comput Biol. 2023;19:e1011572.
21. Alekseichuk I, Wischnewski M, Opitz A. A minimum effective dose for (transcranial) alternating current stimulation. Brain Stimul. 2022;15:1221–2.
22. Nikolin S, Huggins C, Martin D, Alonzo A, Loo CK. Safety of repeated sessions of transcranial direct current stimulation: A systematic review. Brain Stimulation: Basic Translational Clin Res Neuromodulation. 2018;11:278–88.
23. Toth J, Kurtin DL, Brosnan M, Arvaneh M. Opportunities and Obstacles in non-invasive brain stimulation. Front Hum Neurosci. 2024;18:1385427.
24. Toth J, Kurtin DL, Brosnan M, Arvaneh M. Opportunities and Obstacles in non-invasive brain stimulation. Front Hum Neurosci 18, (2024).
25. Opitz A, et al. On the importance of precise electrode placement for targeted transcranial electric stimulation. NeuroImage. 2018;181:560–7.
26. Woods AJ, Bryant V, Sacchetti D, Gervits F, Hamilton R. Effects of electrode drift in transcranial direct current stimulation. Brain Stimul. 2015;8:515–9.
27. Thomas Yeo BT, et al. The organization of the human cerebral cortex estimated by intrinsic functional connectivity. J Neurophysiol. 2011;106:1125–65.
28. Fox MD et al. The human brain is intrinsically organized into dynamic, anticorrelated functional networks. *Proceedings of the National Academy of Sciences* 102, 9673–9678 (2005).
29. Uddin LQ, Kelly C, Biswal AM, Castellanos BBX, F., Milham. M. P. Functional connectivity of default mode network components: Correlation, anticorrelation, and causality. Hum Brain Mapp. 2008;30:625–37.
30. Indahlastari A, et al. Methods to monitor accurate and consistent electrode placements in conventional transcranial electrical stimulation. Brain Stimulation: Basic Translational Clin Res Neuromodulation. 2019;12:267–74.
31. Jog M, et al. A novel technique for accurate electrode placement over cortical targets for transcranial electrical stimulation (tES) clinical trials. J Neural Eng. 2021;18:056049.
32. Fröhlich T, Sindram J, Haueisen J, Hunold A. Force measurement of electrodes on a human head model. tm - Technisches Messen. 2021;88:724–30.
33. Mansouri F et al. Development and validation of a 3D-printed neuronavigation headset for therapeutic brain stimulation. J Neural Eng 15, (2018).
34. Cappon D et al. Tele-supervised home-based transcranial alternating current stimulation (tACS) for alzheimer's disease: a pilot study. Front Hum Neurosci 17, (2023).
35. Charvet LE, Shaw MT, Bikson M, Woods AJ, Knotkova H. Supervised transcranial direct current stimulation (tDCS) at home: A guide for clinical research and practice. Brain Stimulation: Basic Translational Clin Res Neuromodulation. 2020;13:686–93.
36. Wunder S, et al. Novel bifunctional cap for simultaneous electroencephalography and transcranial electrical stimulation. Sci Rep. 2018;8:7259.
37. Sobral M, Guiomar R, Martins V, Ganho-Ávila A. Home-based transcranial direct current stimulation in dual active treatments for symptoms of depression and anxiety: A case series. Front Psychiatry 13, (2022).
38. Kwon S, et al. At-home wireless sleep monitoring patches for the clinical assessment of sleep quality and sleep apnea. Sci Adv. 2023;9:eadg9671.
39. Krainc D, et al. Shifting the trajectory of therapeutic development for neurological and psychiatric disorders. Sci Transl Med. 2023;15:eadg4775.
40. Khambhati AN, Shafi A, Rao VR, Chang EF. Long-term brain network reorganization predicts responsive neurostimulation outcomes for focal epilepsy. Sci Transl Med. 2021;13:eabf6588.
41. Frontiers | Editorial. Combined EEG in research and diagnostics: Novel perspectives and improvements. https://www.frontiersin.org/journals/neuroscience/articles/10.3389/fnins.2023.1152394/full.
42. Haslacher D, Reber P, Soekadar S. Targeting alpha oscillations using closed-loop transcranial alternating current stimulation. Brain Stimulation: Basic Translational Clin Res Neuromodulation. 2023;16:235.
43. Paunovic D, et al. TOWARDS UNDERSTANDING THE NEURAL UNDERPINNINGS OF ASSOCIATIVE MEMORY: A TES-EEG STUDY. IBRO Neurosci Rep. 2023;15:S879.
44. Caravati E, Barbeni F, Chiarion G, Raggi M, Mesin L. Closed-Loop transcranial electrical neurostimulation for sustained attention enhancement: A pilot study towards personalized intervention strategies. Bioengineering. 2024;11:467.
45. Al Qasem W, Abubaker M, Pilátová K, Ježdík P, Kvašňák E. Improving working memory by electrical stimulation and cross-frequency coupling. Mol Brain. 2024;17:72.
46. Dhaynaut M, et al. Impact of 40Hz transcranial alternating current stimulation on cerebral Tau burden in patients with alzheimer's disease: A case series. J Alzheimer's Disease. 2022;85:1667–76.
47. Woods AJ, et al. A technical guide to tDCS, and related non-invasive brain stimulation tools. Clin Neurophysiol. 2016;127:1031–48.
48. Driscoll N, et al. MXene-infused bioelectronic interfaces for multiscale electrophysiology and stimulation. Sci Transl Med. 2021;13:eabf8629.
49. Wang C, et al. On-skin paintable biogel for long-term high-fidelity electroencephalogram recording. Sci Adv. 2022;8:eabo1396.
50. Lopez-Gordo MA, Sanchez-Morillo D, Valle FP, Dry. EEG Electrodes Sensors. 2014;14:12847–70.
51. Mullen TR, et al. Real-Time neuroimaging and cognitive monitoring using wearable dry EEG. IEEE Trans Biomed Eng. 2015;62:2553–67.
52. Heijs JJA, Havelaar RJ, Fiedler P, van Wezel RJA, Heida T. Validation of soft multipin dry EEG electrodes. Sensors. 2021;21:6827.
53. Gao K-P, Yang H-J, Wang X-L, Yang B, Liu J-Q. Soft pin-shaped dry electrode with bristles for EEG signal measurements. Sens Actuators A: Phys. 2018;283:348–61.
54. Węglarczyk S. Kernel density Estimation and its application. ITM Web Conf. 2018;23:00037.
55. Yao D, et al. Which reference should we use for EEG and ERP practice? Brain Topogr. 2019;32:530–49.
56. Tallgren P, Vanhatalo S, Kaila K, Voipio J. Evaluation of commercially available electrodes and gels for recording of slow EEG potentials. Clin Neurophysiol. 2005;116:799–806.
57. Lazanas AC, Prodromidis MI. Electrochemical impedance spectroscopya tutorial. ACS Meas Sci Au. 2023;3:162–93.
58. Bikson M, et al. Safety of transcranial direct current stimulation: evidence based update 2016. Brain Stimulation: Basic Translational Clin Res Neuromodulation. 2016;9:641–61.
59. Goyal K, Borkholder DA, Day SW. Dependence of skin-Electrode contact impedance on material and skin hydration. Sensors. 2022;22:8510.
60. Bera TK. Bioelectrical impedance and the frequency dependent current conduction through biological tissues: A short review. IOP Conf Ser : Mater Sci Eng. 2018;331:012005.
61. Stahn A, Terblanche E, Gunga H-C. Use of bioelectrical impedance: general principles and overview. In: Preedy VR, editor. Handbook of anthropometry: physical measures of human form in health and disease. New York, NY: Springer; 2012. pp. 49–90. https://doi.org/10.1007/978-1-4419-1788-1_3.
62. Rodgers G, et al. Increasing target engagement via customized electrode positioning for personalized transcranial electrical stimulation: A biophysical modeling study. NeuroImage. 2025;311:121206.
63. Soleimani G, et al. Closing the loop between brain and electrical stimulation: towards precision neuromodulation treatments. Transl Psychiatry. 2023;13:1–17.
64. Kasten FH, Duecker K, Maack MC, Meiser A, Herrmann CS. Integrating electric field modeling and neuroimaging to explain inter-individual variability of tACS effects. Nat Commun. 2019;10:5427.
65. Kranjc M, Miklavčič D. Electric field distribution and electroporation threshold. Handbook of electroporation. Cham: Springer International Publishing; 2017. pp. 1043–58. https://doi.org/10.1007/978-3-319-32886-7_4.
66. Guttmann-Flury E, Sheng X, Zhu X. Channel selection from source localization: A review of four EEG-based brain–computer interfaces paradigms. Behav Res. 2023;55:1980–2003.
67. Akalin Acar Z, Makeig S. Effects of forward model errors on EEG source localization. Brain Topogr. 2013;26:378–96.
68. Pinte C, Fleury M, Maurel P. Deep Learning-Based localization of EEG electrodes within MRI acquisitions. Front Neurol 12, (2021).
69. Jc M, Aw T, A, E., P, F., J L. A probabilistic atlas of the human brain: theory and rationale for its development. The International Consortium for Brain Mapping (ICBM). *NeuroImage* 2, (1995).
70. Yang Z, et al. Brain aging patterns in a large and diverse cohort of 49,482 individuals. Nat Med. 2024;30:3015–26.
71. Billot B et al. Robust machine learning segmentation for large-scale analysis of heterogeneous clinical brain MRI datasets. *Proceedings of the National Academy of Sciences* 120, e2216399120 (2023).
72. Missey F, et al. Non-invasive Temporal interference stimulation of the hippocampus suppresses epileptic biomarkers in patients with epilepsy: biophysical differences between Kilohertz and amplitude modulated stimulation. MedRxiv. 2025;2024120524303799. https://doi.org/10.1101/2024.12.05.24303799.

73. Lamoš M, et al. Noninvasive Temporal interference stimulation of the subthalamic nucleus in parkinson's disease reduces beta activity. Mov Disord. 2025;40:1051–60.
74. Saturnino GB, et al. SimNIBS 2.1: A comprehensive pipeline for individualized electric field modelling for transcranial brain stimulation. In: Makarov S, Horner M, Noetscher G, editors. Brain and human body modeling: computational human modeling at EMBC 2018. Cham: Springer International Publishing; 2019. pp. 3–25. https://doi.org/10.1007/978-3-030-21293-3_1.
75. Fischl B. FreeSurfer NeuroImage. 2012;62:774–81.
76. Saturnino GB, Madsen KH, Thielscher A. Electric field simulations for transcranial brain stimulation using FEM: an efficient implementation and error analysis. J Neural Eng. 2019;16:066032.
77. Sullivan CB, Kaszynski AA. PyVista: 3D plotting and mesh analysis through a streamlined interface for the visualization toolkit (VTK). J Open Source Softw. 2019;4:1450.
78. Waskom ML. Seaborn: statistical data visualization. J Open Source Softw. 2021;6:3021.

Publisher's note